BMC Cancer

RESEARCH Open Access

Prediction of pathological complete response to neoadjuvant chemoimmunotherapy in non–small cell lung cancer using ^{18}F-FDG PET radiomics features of primary tumour and lymph nodes

Xingbiao Liu[1,3,4], Zhilin Ji[2], Libo Zhang[1,3,4], Linlin Li[1,3,4], Wengui Xu[1,3,4*] and Qian Su[1,3,4*]

Abstract

Background Predicting the response to neoadjuvant chemoimmunotherapy in patients with resectable non-small cell lung cancer (NSCLC) facilitates clinical treatment decisions. Our study aimed to establish a machine learning model that accurately predicts the pathological complete response (pCR) using ^{18}F-FDG PET radiomics features.

Methods We retrospectively included 210 patients with NSCLC who completed neoadjuvant chemoimmunotherapy and subsequently underwent surgery with pathological results, categorising them into a training set of 147 patients and a test set of 63 patients. Radiomic features were extracted from the primary tumour and lymph nodes. Using 10-fold cross-validation with the least absolute shrinkage and selection operator method, we identified the most impactful radiomic features. The clinical features were screened using univariate and multivariate analyses. Machine learning models were developed using the random forest method, leading to the establishment of one clinical feature model, one primary tumour radiomics model, and two fusion radiomics models. The performance of these models was evaluated based on the area under the curve (AUC).

Results In the training set, the three radiomic models showed comparable AUC values, ranging from 0.901 to 0.925. The clinical model underperformed, with an AUC of 0.677. In the test set, the Fusion_LN1LN2 model achieved the highest AUC (0.823), closely followed by the Fusion_Lnall model with an AUC of 0.729. The primary tumour model achieved a moderate AUC of 0.666, whereas the clinical model had the lowest AUC at 0.631. Additionally, the Fusion_LN1LN2 model demonstrated positive net reclassification improvement and integrated discrimination improvement values compared with the other models, and we employed the SHapley Additive exPlanations methodology to interpret the results of our optimal model.

*Correspondence:
Wengui Xu
wenguixy@yeah.net
Qian Su
suqian@tjmuch.com

Full list of author information is available at the end of the article

Conclusions Our fusion radiomics model, based on ^{18}F-FDG-PET, will assist clinicians in predicting pCR before neoadjuvant chemoimmunotherapy for patients with resectable NSCLC.

Keywords Non-small cell lung cancer, Radiomics, Neoadjuvant chemoimmunotherapy, Pathological response, PET

Background

Immune checkpoint inhibitors (ICIs) have revolutionised the treatment of non-small cell lung cancer (NSCLC) [1]. Numerous studies have confirmed that immunotherapy improves survival in patients with advanced-stage NSCLC [2, 3]. Similarly, research on the application of immunotherapy in early stages is rapidly growing, paralleling investigations in advanced diseases [4]. Neoadjuvant treatment not only reduces tumour size before surgery but also enhances systemic antitumor T-cell priming, thereby eradicating micrometastatic cancer and preventing postsurgical relapse [5–7]. The IMpower010 and PEARLS/KEYNOTE-091 trials illustrated a benefit in disease-free survival in stage I–III patients treated with ICIs, although the overall survival data are still not fully understood [8, 9]. Consistent correlations have been observed between pathological responses and survival outcomes in neoadjuvant chemoimmunotherapy clinical trials [10–12]. By utilising surrogate endpoint indicators, such as major pathological response (MPR) and pathological complete response (pCR), the efficacy of neoadjuvant chemoimmunotherapy can be assessed earlier, potentially facilitating the discovery of new prognostic biomarkers [4, 13, 14].

Many reports have suggested that invasive biomarkers such as programmed death-ligand 1 (PD-L1) expression, tumour-infiltrating lymphocytes, and tumour mutational burden can predict patient response to neoadjuvant therapy [15–18]. Therefore, there is an urgent need to explore alternative non-invasive predictive biomarkers for neoadjuvant chemoimmunotherapy.

^{18}F-FDG PET/CT is indispensable for the evaluation of NSCLC, encompassing various dimensions, such as tumour detection, disease staging, treatment response assessment, and prognosis evaluation [19]. ^{18}F-FDG PET/CT images provide anatomical and metabolic views of tumours and show great promise for guiding immunotherapy in patients with NSCLC [20, 21]. Giulia et al. reported that baseline ^{18}F-FDG PET/CT before immunotherapy may effectively predict the response to chemoimmunotherapy, observing a significant relationship between metabolic semi-quantitative parameters of primary tumours and progression-free disease (PD) [22]. Tao et al. further presented the clinical significance of post-treatment percentage changes in metabolic parameters using ^{18}F-FDG PET as a promising biomarker for predicting early-phase clinical outcomes [23]. Radiomics aims to create more accurate predictive models for evaluating patient pathological responses and prognosis by extracting high-dimensional quantitative features beyond traditional visual analysis [24–26]. Wang et al. used pretreatment CT radiomic features as a non-invasive tool to predict MPR in NSCLC after neoadjuvant chemoimmunotherapy, achieving an area under the curve (AUC) of 0.60 [27].

However, patients with resectable NSCLC comprise a highly diverse group, encompassing those with stage I–II tumours and some locally advanced stage III tumours. A significant number of these patients exhibit varying degrees of mediastinal lymph node (LN) involvement. PET information extracted from metastatic LNs has been shown to have a greater prognostic value than that extracted from the primary tumour alone, providing additional valuable insights [28].

Therefore, our study aimed to develop and validate a radiomics model that accurately predicts pCR in patients with NSCLC receiving neoadjuvant chemoimmunotherapy. This model leverages ^{18}F-FDG-PET images of primary tumours and mediastinal LN metastases and offers a novel and practical approach with certain application prospects in medical research.

Methods

Patient population

The study was approved by the Ethics Committee of Tianjin Medical University Cancer Hospital (bc20241623). The study was conducted in accordance with the ethical principles outlined in the Declaration of Helsinki. The need for informed consent was waived by the ethics committee due to the retrospective study design. We conducted a retrospective analysis to gather clinicopathological data from 210 patients diagnosed with NSCLC through pathological confirmation and treated with neoadjuvant chemoimmunotherapy at the Tianjin Cancer Hospital between November 2018 and May 2024. The inclusion criteria encompassed: (a) patients with potentially operable stage Ib-IIIb NSCLC, diagnosed via image-guided or bronchoscopy-guided biopsy; (b) individuals without common driver gene EGFR mutations; (c) those with no prior history of other tumours or antitumor therapies; (d) patients who underwent at least two doses of immunotherapy-based neoadjuvant treatment and were scheduled for surgery; (e) patients who underwent whole-body PET-CT scans within 2 weeks before neoadjuvant chemoimmunotherapy. Figure 1 outlines the exclusion criteria. Following this, patients were subsequently randomised into a training group (for the development and refinement of the radiomics model)

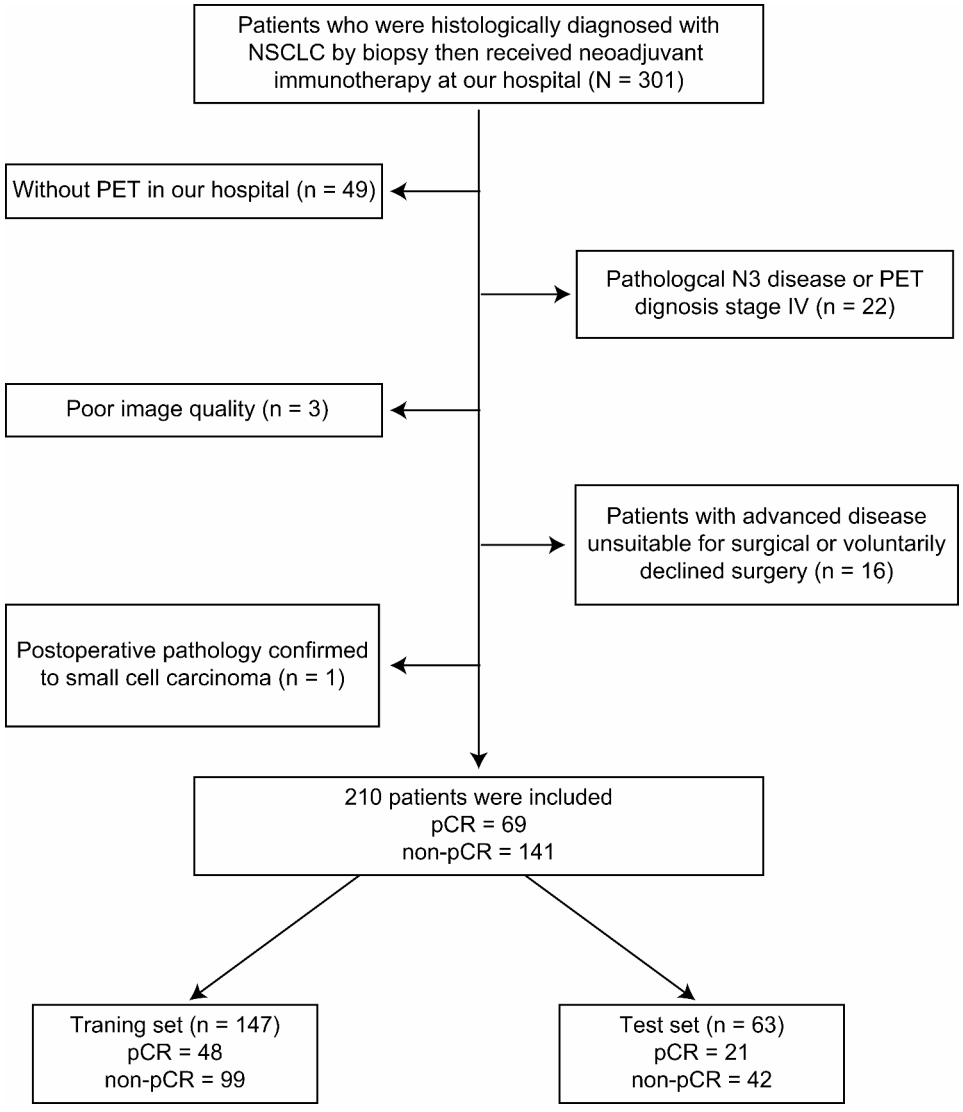

Fig. 1 Patients' inclusion flowchart and datasets partition

and a test group (for the comprehensive validation of the model's predictive capabilities) at a 7:3 ratio.

Pathological information

Preoperative pathology was primarily ascertained through lung or bronchoscopy biopsies, and all external biopsy cases were revalidated by our pathologists. The assessments included routine immunohistochemistry and genetic testing for EGFR mutations. The postoperative pathology was confirmed by examining surgical resection samples collected after neoadjuvant chemotherapy. The pCR was determined by the absence of any viable tumour cells in all examined slides of the primary tumour tissue and LNs.

PET and CT scan protocol

The enrolled patients underwent PET/CT using two scanners: General Electric Discovery Elite and General Electric ST4. Before the ^{18}F-FDG PET scan, patients were instructed to fast for at least 6 h to ensure that their blood glucose levels were below 11.1 mmol/L. Subsequently, the radioactive drug ^{18}F-FDG was administered intravenously at a dosage of 4.2 MBq/kg. The patients were then instructed to rest in a dark, quiet environment. Image acquisition was performed 50–60 min later. The CT scanning protocols were set at 120 kVp and 80 mAs with a slice thickness of 3.75 mm. Low-dose CT images were used for attenuation correction. For PET imaging, scans were obtained in the three-dimensional mode with eight-bed positions, each lasting 2.5 min, and subsequently reconstructed using the OSEM algorithm. The

PET and CT images covered the area from the vertex to the proximal leg.

Image reconstruction and segmentation

To minimise variations arising from differences in the reconstruction layer thicknesses and pixel sizes, all CT and PET images were uniformly resampled to a voxel size of 1 mm × 1 mm × 1 mm, and the PET images were normalised to a grayscale range spanning from 0 to 40. Owing to the low-dose CT scanning, these CT images served merely as an aid in contouring the target regions on the PET images and were not used for extracting radiomic features to develop models. The clinical standard for evaluating LNs in imaging is to classify them as positive for metastasis when the PET maximum standardised uptake value (SUVmax) is ≥ 2.5 and the short-axis diameter on CT is more than 1 cm [29, 30]. The volumes of interest (VOIs) underwent semiautomatic segmentation using 3D Slicer, a sophisticated imaging post-processing software. For primary tumours and LNs, delineation was performed using a fixed threshold of 2.5 [31, 32]. Subsequently, manual corrections were performed to refine the delineation and exclude any negative normal tissues. Thirty PET images were randomly selected for repeated contouring, and features with ICC values above 0.70 were retained for further screening. To examine the existence of heterogeneity among LNs located in distinct stations, our subsequent studies used 'individualised' and 'aggregated' delineation techniques for the N1 and N2 stations within the mediastinum [33, 34]. Consequently, two unique combinations are derived to formulate the fusion model. This segmentation process was executed by two independent radiologists, each with 5 years of experience in chest interpretation. Disagreements between the two radiologists were resolved through consultation with a senior expert radiologist with 10 years of experience in imaging diagnosis.

Segmentation and radiomics feature extraction

The PyRadiomics open-source Python package (version 3.7.) was used to extract a range of features, including shape features ($n = 14$), first-order features ($n = 396$), and texture analysis features ($n = 1606$). A comprehensive set of features available in PyRadiomics was derived from the original and filtered images by incorporating the wavelet and Laplacian of Gaussian transformations. Consequently, 2016 features were extracted for each region across all segmentation methods. Furthermore, gray-level discretisation with a fixed bin width (0.25) was applied to the PET images using PyRadiomics.

Radiomics feature fusion and selection

Initially, the imaging features across various dimensions were subjected to Z-score normalisation, standardising the data to have a mean of 0 and a standard deviation of 1. We combined the features of the primary tumours and metastatic LNs using early fusion techniques, thereby merging them into new comprehensive feature vectors. Feature fusion was performed by using the maximum aggregation method. We established one group of primary tumour features and two groups of fusion features. Pearson's rank correlation was used to eliminate features with correlation coefficients > 0.9. Ultimately, we employed the least absolute shrinkage and selection operator (LASSO) logistic regression to further refine our features, determining the optimal regularisation parameter λ through 10-fold cross-validation to minimise binomial deviance. Using these features selected from the training dataset, we constructed machine learning models and evaluated their performances across different imaging modalities.

Radiomics model development

After utilising LASSO for feature selection, we developed risk models using a random forest machine-learning algorithm. The implementation of the machine learning algorithms was facilitated using Scikit-learn version 1.0.2. Subsequently, we established one clinical model, one Primary _ Tumour radiomics model, and two fusion radiomics models, naming them 'Clinic model', 'Primary_Tumour model', 'Fusion_LNall model', and 'Fusion_LN1LN2 model'. Finally, we conducted a comparative analysis to evaluate the performance of each model.

Statistical analysis

All statistical analyses were performed using Python version 3.7.12. The Shapiro–Wilk test was used to verify the normality of the clinical features. Based on their distribution characteristics, continuous variables were compared using either a T test or a Mann-Whitney U test, whereas categorical variables were evaluated with Chi-square (χ^2) tests. Table 1 provides a detailed overview of the baseline characteristics of all cohorts involved. The diagnostic accuracy of our model was rigorously evaluated using ROC curves within a designated test set. Additionally, we assessed the clinical utility of our predictive models using the DeLong test, decision curve analysis (DCA), net reclassification improvement (NRI) and integrated discrimination improvement (IDI). Figure 2 presents a flowchart outlining this procedure.

Results

Clinical characteristics

Table 1 shows the clinical characteristics of the 210 patients with NSCLC, with p-values indicating statistical significance. Among them, 69 (32.9%) were classified as pCR and 141 (67.1%) were classified as non-pCR. Patients were randomly assigned to a training set (147

Table 1 Clinical characteristics of patients

Characteristics	Total (*n* = 210)	Training sets (*n* = 147)	Test sets (*n* = 63)	*p*-value
Age	61.04 ± 6.71	61.05 ± 6.79	61.02 ± 6.57	0.974
Sex (*n*, %)				0.217
Male	184(87.62)	132(89.80)	52(82.54)	
Female	26(12.38)	15(10.20)	11(17.46)	
Histological type (*n*, %)				0.253
SQCC	144(68.57)	102(69.39)	42(66.67)	
ADA	52(24.76)	33(22.45)	19(30.16)	
Others	14(6.67)	12(8.16)	2(3.17)	
cT stage (*n*, %)				0.117
cT1	25(11.90)	13(8.84)	12(19.05)	
cT2	97(46.19)	67(45.58)	30(47.62)	
cT3	53(25.24)	39(26.53)	14(22.22)	
cT4	35(16.67)	28(19.05)	7(11.11)	
cN stage (*n*, %)				0.669
cN0	83(39.52)	61(41.50)	22(34.92)	
cN1	49(23.33)	33(22.45)	16(25.40)	
cN2	78(37.14)	53(36.05)	25(39.68)	
Clinical stage (*n*, %)				0.834
I	10(4.76)	7(4.76)	3(4.76)	
II	77(36.67)	52(35.37)	25(39.68)	
III	123(58.57)	88(59.86)	35(55.56)	
Smoke (*n*, %)				0.486
Current or former	171(81.43)	122(82.99)	49(77.78)	
Never	39(18.57)	25(17.01)	14(22.22)	

SQCC, Squamous Cell Carcinoma; ADA, Adenocarcinoma

The pre-NAT clinical stage was assessed using the eighth edition of the TNM Classification system by the International Association for the Study of Lung Cancer (IASLC)

patients, including 48 with pCR) or a test set (63 patients, including 21 with pCR). No clinically significant differences in characteristics were observed between the two groups.

As shown in Table 2, a comprehensive multivariate analysis was conducted on all clinical features, with emphasis on the calculation of adjusted odds ratios (OR) and corresponding p-values while controlling for potential confounders. For the univariate analysis, 'smoke', 'sex'," histological type ', 'cT stage', 'cN stage', and' clinical stage' have OR of 0.506 (95% confidence interval [CI]: 0.369–0.694), 0.500 (95% CI: 0.369–0.678), 0.562 (95% CI: 0.456–0.694), 0.765 (95% CI: 0.686–0.854), 0.619 (95% CI: 0.491–0.781), and 0.737 (95% CI: 0.658–0.825). The results suggest a protective effect against the outcome for 'smoke', 'sex', 'histological type', and possibly 'cN stage' (depending on the context, as OR < 1 typically indicates a lower risk), whereas 'cT stage' and' clinical stage' suggest a lesser but still statistically significant association ($p < 0.05$ for all). 'Age' has a univariate OR of 0.989 (95% CI: 0.984–0.994, $p < 0.05$) and a multivariate OR of 1.041 (95% CI: 1.011–1.071, $p < 0.05$). Thus, 'age' did not demonstrate a clear and definitive effect, and the effect was very small. In the multivariate analysis, only 'histological type' and 'clinical stage' retained statistical significance with OR of 0.464 (95% CI: 0.263–0.819, $p = 0.026$) and 0.289 (95% CI: 0.121–0.689, $p = 0.019$), respectively, whereas the other features lost their statistical significance.

Radiomics feature extraction and selection

After eliminating redundant radiomic features using the Pearson correlation method, 131, 108, and 103 features were retained from the Primary_Tumour, Fusion_LNall, and Fusion_LN1LN2 VOIs, respectively. Subsequently, using the LASSO method, as illustrated in Fig. 3, to select 20, 6, and 13 highly robust features for training

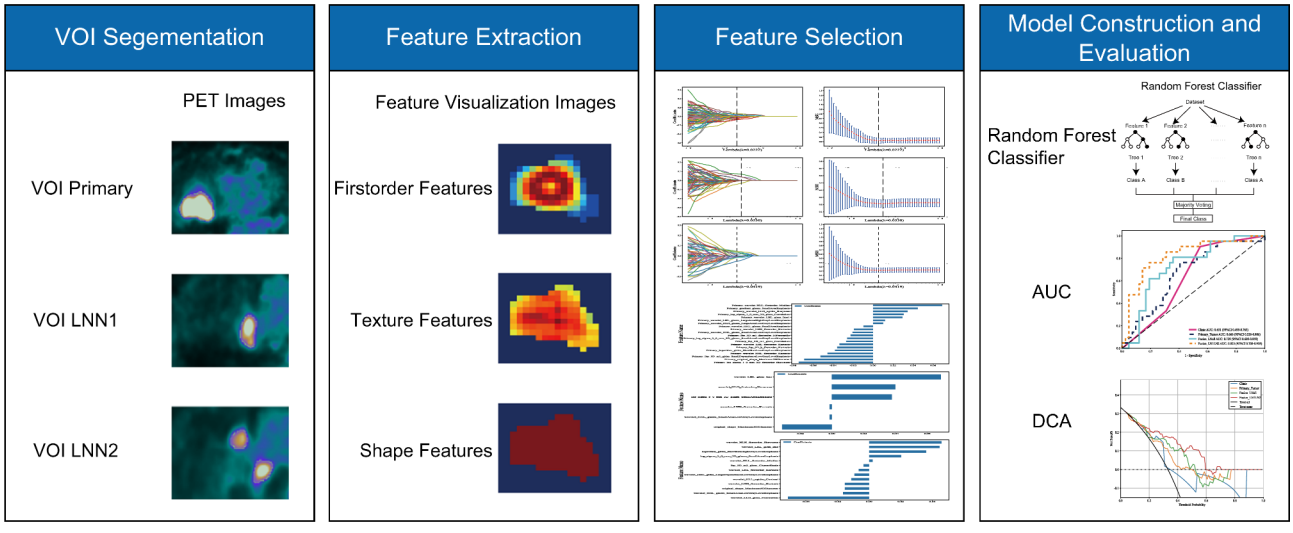

Fig. 2 Flowchart showing the study process

Table 2 Univariate and multivariate analyses of clinical characteristics to predict pCR

Characteristics	Univariate analysis			Multivariate analysis		
	OR	95% CI	*p*-value	OR	95% CI	*p*-value
Age	0.989	0.984–0.994	< 0.001	1.041	1.011–1.071	0.021
Sex	0.5	0.369–0.678	< 0.001	1.093	0.339–3.522	0.9
Histological type	0.562	0.456–0.694	< 0.001	0.464	0.263–0.819	0.026
cT stage	0.765	0.686–0.854	< 0.001	1.226	0.761–1.974	0.482
cN stage	0.619	0.491–0.781	0.001	1.671	0.919–3.04	0.158
Clinical stage	0.737	0.658–0.825	< 0.001	0.289	0.121–0.689	0.019
Smoke	0.506	0.369–0.694	< 0.001	0.872	0.324–2.347	0.82

The clinical characteristics with p-values are listed in the table

the models corresponding to these regions. The features selected for all the radiomics models are presented in Fig. 4.

Predictive performance of clinic model

Significant features identified through multivariate screening were incorporated into the construction of the clinical signature of the Clinic model, and we developed a random forest machine learning model using the selected clinical features. The clinical model revealed the lowest AUC values across both sets (Fig. 5), with 0.677 and 0.631 in the training and test sets, respectively.

Predictive performance of different models

Using the most distinctive imaging features from the primary tumour and LN regions, we constructed a primary tumour model and two fusion models using a random forest machine learning algorithm. The predictive performance of each model is summarised in Table 3. Among all the training sets, the AUCs of the different radiomics models for predicting pCR ranged from 0.901 to 0.925. In the test set, the Primary_Tumour model performed normally with an AUC of 0.666. In addition, the AUCs of the different fusion models were even higher, reaching 0.729 and 0.823, respectively. Notably, the Fusion_LN1LN2 model exhibits the highest AUC and accuracy scores.

The predictive capabilities of the various models for pCR are presented in Table 3, and the fusion models with higher predictive values than the primary tumour models are depicted in Fig. 5. The statistical significance of the differences among the various models was evaluated using the DeLong test on both datasets. As shown in Fig. 6, the predictive ability of the Fusion_LN1LN2 model for pCR was significantly improved compared to that of the Primary_Tumour model and clinical model in the Delong test. Figure 7 shows the calibration curves for the training and test sets. Figure 8 presents the DCA for the test set, with significant net gains observed for the Fusion_LN1LN2 model. Figure 9 presents the NRI and IDI for the test set, with the net gains observed for the Fusion_LN1LN2 model.

Interpretation of machine learning model

In Fig. 10, the SHapley Additive exPlanations (SHAP) summary scatter plot shows how the Fusion_LN1LN2 random forest model works, visualising the model's interpretation and illustrating the relationship between prediction parameters and predicted probabilities through colour variation. The top variables had more predictive power and were more important to the model than the bottom variables. In Fig. 11, the waterfall and force plots display all features in the order of their contribution to the final pCR output, with the direction of each contribution indicated by colour. Blue indicates negative contributions, meaning that the feature diminishes the prediction value, whereas red indicates positive contributions, indicating that the feature enhances the prediction value. After summing up all the feature contributions, if the resultant value surpasses the base value $E[f(z)] = 0.305$, the patient is deemed to have achieved pCR; otherwise, the patient is considered to be non-pCR.

Discussion

Univariate analysis revealed that smoking, sex, histological type, cN stage, clinical stage, and cT stage were significantly associated with pCR. However, in multivariate analysis, only 'histological type' and 'clinical stage' maintained statistical significance, suggesting that they were independent predictors of achieving pCR. The loss of significance for other features in the multivariate model may indicate that their associations are confounded by other variables or that their effects are not independent. The clinical model integrated with the selected clinical characteristics illustrated the lowest AUC values across both sets, with 0.677 in the training set and 0.631 in the test set. We employ radiomics models based on ^{18}F-FDG-PET imaging as the non-invasive biomarker to predict the effectiveness of neoadjuvant chemoimmunotherapy in patients with stage IB-IIIB NSCLC. Our findings indicated that all models can potentially predict the pCR status of patients with NSCLC, with the Fusion_LN1LN2 model demonstrating the best predictive performance. It achieved AUC values of 0.903 in the training set and 0.823 for the test set and attained the highest accuracy

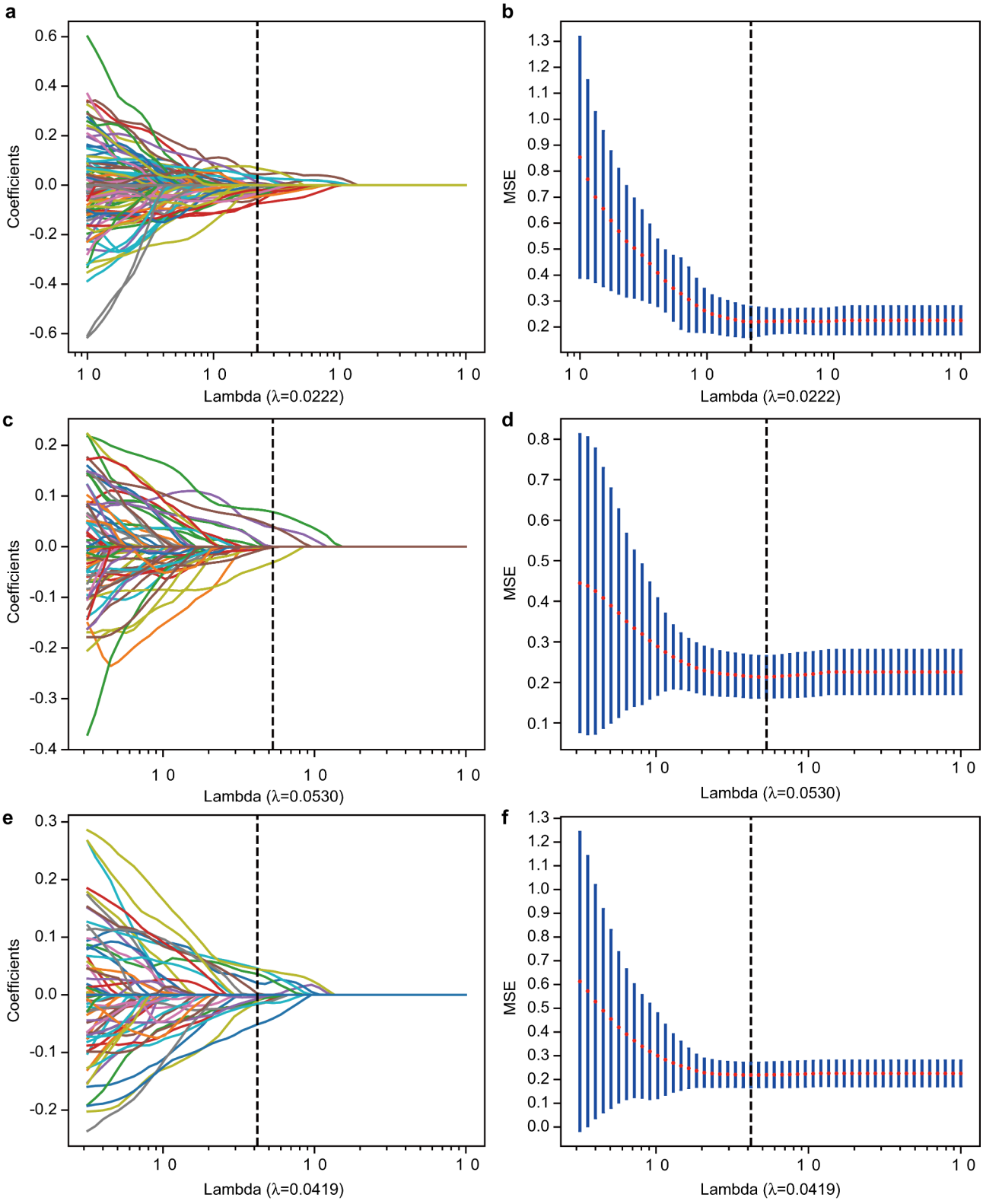

Fig. 3 The radiomics feature selection process was conducted in the Primary_ Tumor VOI (**A**, **B**), Fusion_LNall VOI (**C**, **D**), and Fusion_LN1LN2 VOI (**E**, **F**). The optimal parameter λ was identified with tenfold cross-validation

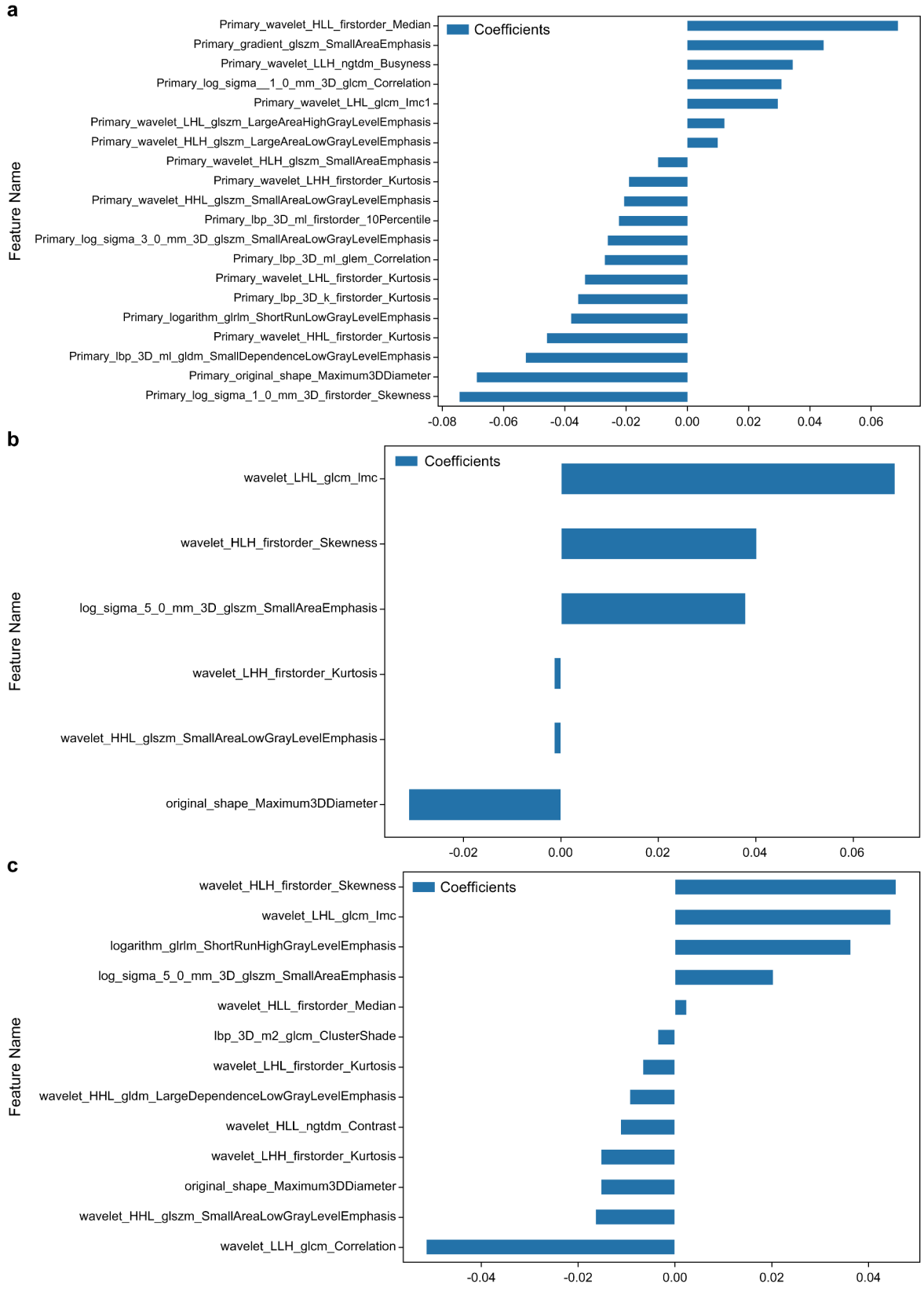

Fig. 4 Radiomics features selected for the Primary_Tumour model (**A**), Fusion_LNall model (**B**), and Fusion_LN1LN2 model (**C**)

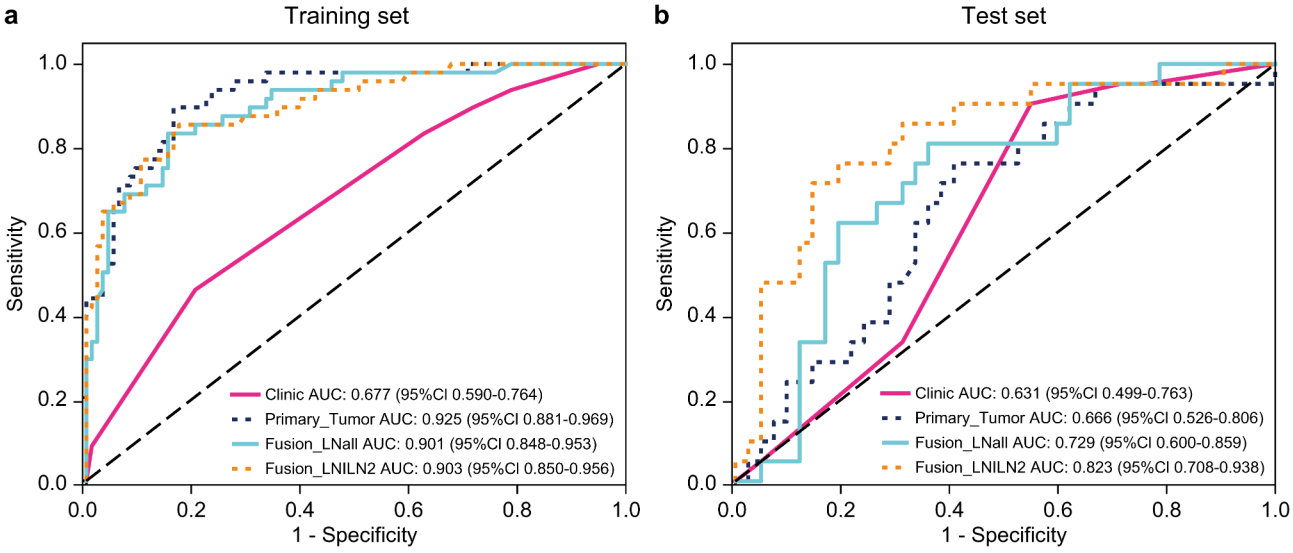

Fig. 5 The ROC curves of the random forest machine learning models in the training set (**A**) and test set (**B**)

Table 3 Discrimination performance of predict models for predicting pCR status in patients with NSCLC

Model name	Set	ACC	AUC (95% CI)	SEN	SPE	PPV	NPV	F1
Primary_Tumour	**Training**	0.850	0.925(0.881–0.969)	0.875	0.838	0.724	0.933	0.792
Primary_Tumour	**Test**	0.635	0.666(0.526–0.806)	0.714	0.595	0.469	0.806	0.566
Fusion_LNall	**Training**	0.837	0.901(0.848–0.953)	0.812	0.848	0.722	0.903	0.765
Fusion_LNall	**Test**	0.683	0.729(0.600–0.859)	0.762	0.643	0.516	0.844	0.615
Fusion_LN1LN2	**Training**	0.830	0.903(0.850–0.956)	0.833	0.828	0.702	0.911	0.762
Fusion_LN1LN2	**Test**	0.794	0.823(0.708–0.937)	0.667	0.857	0.7	0.837	0.683
Clinic	**Training**	0.694	0.677(0.590–0.764)	0.083	0.99	0.8	0.69	0.151
Clinic	**Test**	0.571	0.631(0.499–0.763)	0.333	0.69	0.35	0.674	0.341

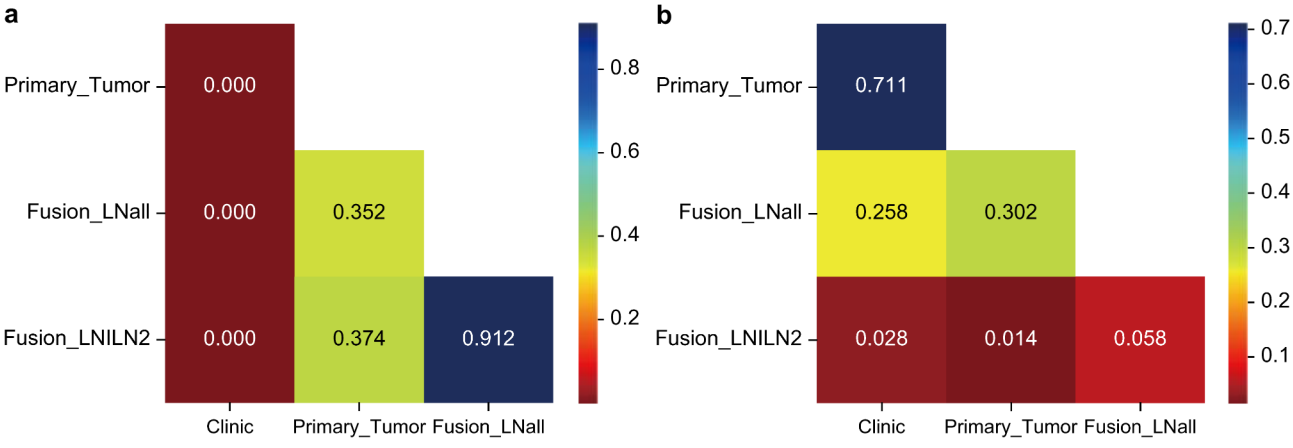

Fig. 6 The results of the DeLong test for comparing random forest models in the training set (**A**) and test set (**B**). The Fusion_LN1LN2 model demonstrated a significant improvement over the Primary_Tumour models and Clinic model in the test set

score of 0.794. In the test set, the Fusion_LN1LN2_model achieved positive NRI and IDI values compared with the other models.

Neoadjuvant chemoimmunotherapy has recently garnered significant attention for treating resectable NSCLC. Compared to chemoradiotherapy and targeted therapy, it notably reduces tumour size and offers patients greater survival benefits. The robust and consistent association observed between pathological response and survival following neoadjuvant therapy supports pCR or MPR as surrogate endpoints for overall survival in patients with resectable NSCLC undergoing neoadjuvant treatment [35]. A clinical trial of sintilimab exhibited a 16.2% pCR rate in patients with stage IA–IIIB NSCLC

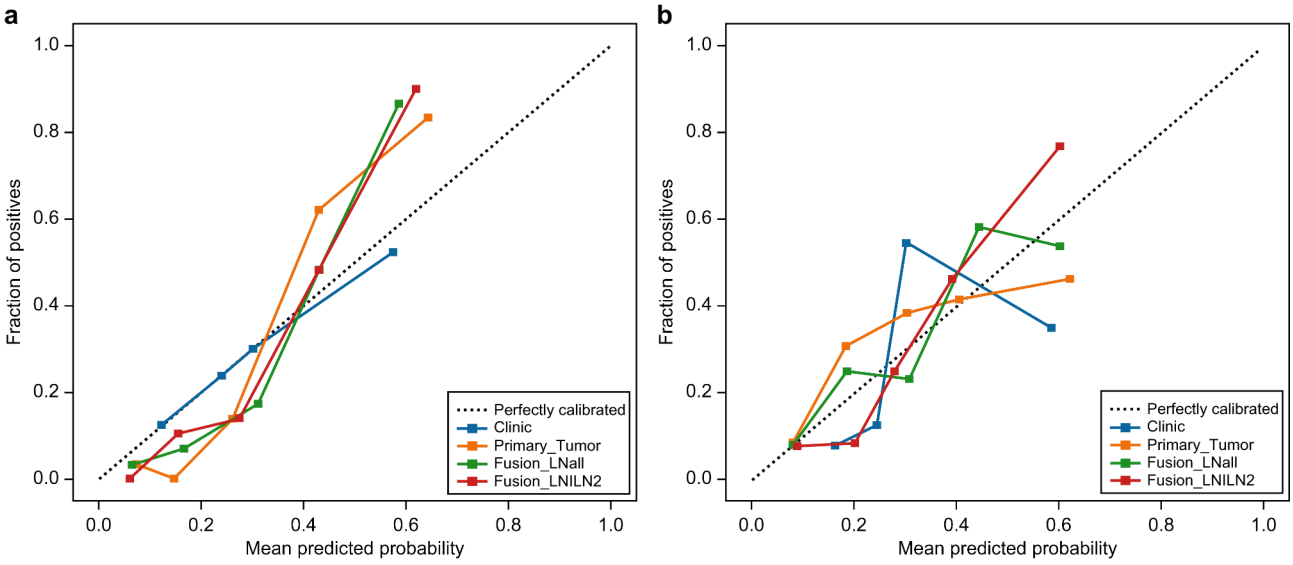

Fig. 7 Calibration curves of different random forest machine learning models in the training (**A**) and test set (**B**)

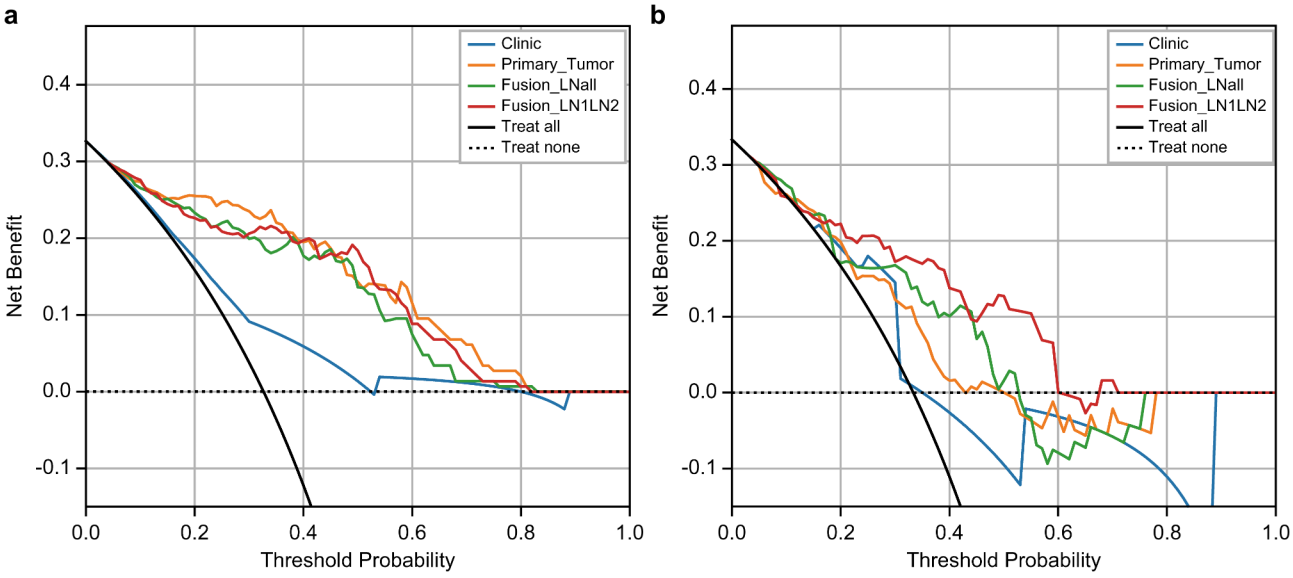

Fig. 8 The decision curve analyses of random forest machine learning models in the training set (**A**) and test set (**B**). The Fusion_LN1LN2 model achieved the greatest net effect in the test set

[36]. A notable additional finding was the significant correlation between SUVmax reduction on PET and the pathological response, underscoring PET's utility in preoperative tumour response assessment and guiding decisions regarding neoadjuvant chemoimmunotherapy. In another trial, combining neoadjuvant atezolizumab with chemotherapy resulted in a 33% pCR rate, an improvement compared with studies using neoadjuvant chemotherapy alone [37]. This rate aligns with our experimental findings. Remarkably, the observed objective responses were independent of PD-L1 expression, indicating that it is not a predictive factor for treatment benefits. Therefore, the identification of predictive biomarkers for response remains a key focus. Consequently, we employed radiomic models as non-invasive biomarkers to predict the effectiveness of neoadjuvant chemoimmunotherapy in patients with resectable NSCLC.

^{18}F-FDG-PET reveals tumour metabolic diversity and is important for evaluating the immunotherapy effectiveness of NSCLC [38]. These parameters effectively predicted pathological response after neoadjuvant chemoimmunotherapy. Zhao et al. observed a significant reduction in SUVmax among 18 patients with MPR following neoadjuvant toripalimab immunotherapy [39]. Similarly, Zhuang et al. determined that ΔSUVmax% and post-therapy SUVmax effectively predicted MPR

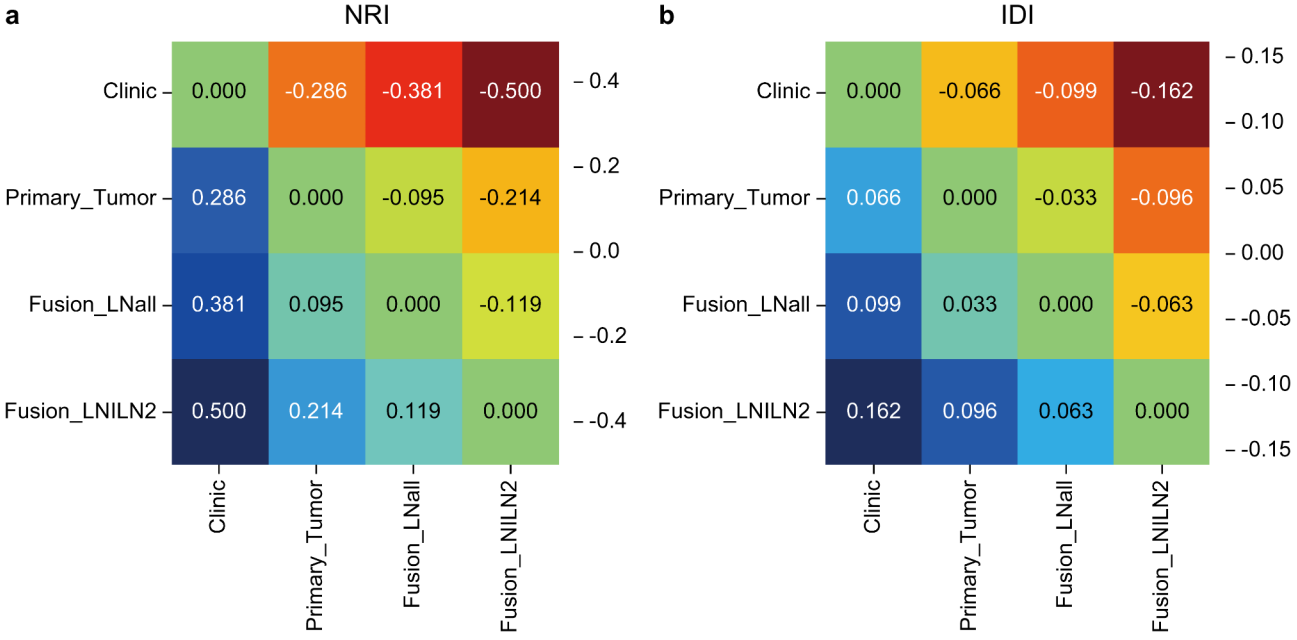

Fig. 9 The Fusion_LN1LN2 model showed net gains in terms of NRI (**A**) and IDI (**B**) compared to the other models in the test set

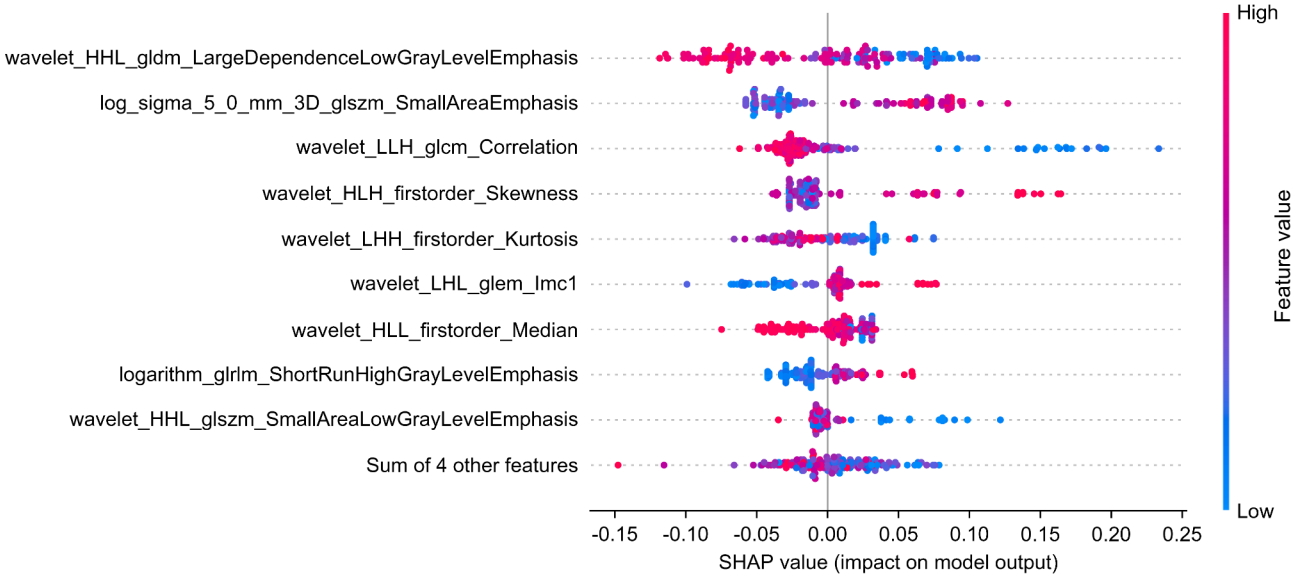

Fig. 10 The summary plots of SHAP values for the Fusion_LN1LN2 model provide a visual representation. They utilise a scatter plot to depict the correlation between radiomics feature values and predicted probabilities, with colours distinguishing between positive and negative predictive effects

and pCR in patients with NSCLC undergoing neoadjuvant chemoimmunotherapy [40]. Furthermore, applying ^{18}F-FDG-PET radiomic features in predicting pCR following neoadjuvant therapy has garnered increasing attention and recognition from a growing body of scholars [41–44]. However, these studies focused only on the radiomic features of the primary tumour, neglecting the potential significance of LN metastasis characteristics. Resectable NSCLC is a highly heterogeneous disease marked by wide differences in tumour volume, local spread, and LN involvement. Although our AUC analysis of the Primary_Tumour model revealed high discriminatory ability in the training set, with a sensitivity and specificity of 0.875 and 0.838, respectively, its performance significantly declined in the test set. This indicates that a model based solely on primary tumour features may not generalise well to the complex and heterogeneous data of patients with stage I–III NSCLC. Therefore, further investigation, extraction, and integration of information from other metastatic sites is necessary.

The CheckMate-816 trial posited that the pathological response of LNs offers supplementary prognostic

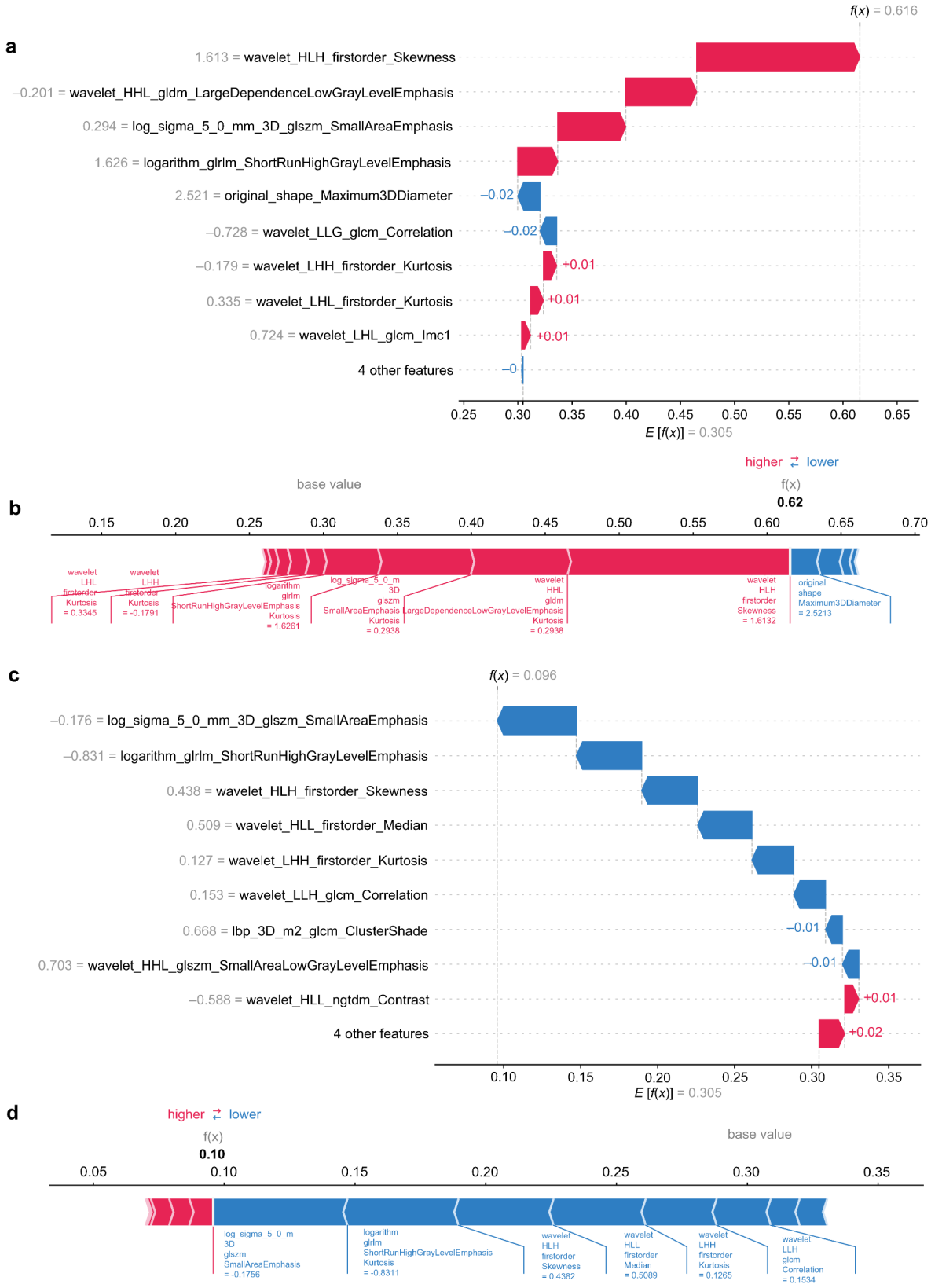

Fig. 11 Waterfall plots (**A**, **C**) and force plots (**B**, **D**) provide SHAP visualisations for the Fusion_LN1LN2 random forest model. (A, B) demonstrate the role of important radiomics features in predicting pCR outcome in a patient with NSCLC. (**C**, **D**) show how these features predict a non-pCR outcome in patients with NSCLC

information beyond that provided by the primary tumour alone [45]. A histopathological assessment revealed that patients undergoing neoadjuvant chemoimmunotherapy with metastatic tumours larger than 4.5 mm in size within the LNs are at an increased risk of recurrence [46]. Therefore, a more comprehensive and precise model of pathological response is needed. PET radiomic signatures extracted from metastatic LNs have been shown to provide a complementary prognostic value to those derived solely from the primary tumour [47, 48]. In our study, we initially evaluated the potential of PET to predict pCR in patients receiving neoadjuvant chemoimmunotherapy using radiomics features extracted from the primary tumour. Subsequently, we constructed a model by integrating the radiomic features of the primary tumour and the LNs. Our study demonstrates that fusion models can significantly enhance prediction accuracy, positive predictive value, and negative predictive value for pCR in patients. We developed two types of fusion models: (1) the Fusion_LNall mode, which collectively extracts features from all mediastinal metastatic LNs as a whole, and (2) the Fusion_LN1LN2 mode, which distinguishes between mediastinal N1 and N2 station LNs and separately extracts radiomics features of metastatic LNs from each other. In the training set, the two radiomics models exhibited comparable AUC values ranging from 0.901 to 0.903. In the test set, the Fusion_LN1LN2model had the highest AUC of 0.823, followed closely by the Fusion_LNall model with an AUC of 0.729. The AUC analysis of specific indicators revealed notable variations in performance among the different models. Patients with stage I–III NSCLC display diverse N stages, and conventional radiomics studies often fail to comprehensively analyse this diverse patient cohort, frequently neglecting the distinct characteristics of metastatic LN lesions. Sara et al. integrated imaging information by combining ^{18}F-FDG-PET radiomic features from primary tumours and LNs, achieving enhanced prognostic discriminatory power for NSCLC [28]. We separately extracted features from various lesion regions and selected the maximum values for the features across these regions. Given that radiomic features often reflect tumour heterogeneity, this method enables us to optimally harness the most heterogeneous imaging data from all tumour lesions. This finding confirms that tumour heterogeneity is present not only in primary tumours and LN metastases but also across different mediastinal LN stations [49, 50]. The 'seed and soil' hypothesis suggests that, given the significant variations in oxygen levels, acidity, and metabolite profiles across different organs and tissues, the tumour microenvironment exhibits regional differences [51]. Despite originating from the same tumour 'seed', unique tumour characteristics emerge, aligning with the organ-specific metabolic 'soil'. Consequently, metabolic patterns in metastatic lesions may diverge from those at the primary tumour site, reflecting this heterogeneity. This is similar to our findings from the PET imaging radiomics studies.

Our Fusion_LN1LN2 model was built by carefully selecting 13 features and combining them using a random forest classifier, thereby significantly enhancing the pCR prediction differentiation performance. To enhance model interpretability, we used SHAP [52]. This method quantifies how each feature affects predictions by measuring its impact on the difference between individual and average model outputs [53, 54]. This provides a clear understanding of the contribution of each feature to the model, making it easier to understand their influence. Key features in our study, such as wavelet_HHL_gldm_LargeDependenceLowGrayLevelEmphasis, log_sigma_5_0_mm_3D_glszm_SmallAreaEmphasis, wavelet_LLH_glcm_Correlation, wavelet_HLH_firstorder_Skewness, and wavelet_LHH_firstorder_Kurtosis, may play a significant role in predicting pCR.

Our study has some limitations. Despite the application of strict inclusion criteria, a selection bias may still exist in this retrospective study. Even with a 5-year data collection period, economic and other practical constraints limited the number of patients eligible for neoadjuvant chemoimmunotherapy who completed baseline PET scans, resulting in a relatively small sample size. Additionally, we did not consider other potentially valuable factors, such as PD-L1 status and tumour-infiltrating lymphocytes. Future research efforts should aim to integrate these factors with radiomic features to enhance prediction accuracy. Finally, the impact of various neoadjuvant chemoimmunotherapy regimens on predictive outcomes requires further exploration, and additional studies are needed to assess the predictive value of 18 F-FDG-PET across different treatment regimens.

Conclusions

This study indicates that the primary tumour-metastatic LN radiomics model can enhance pCR prediction in patients with resectable NSCLC. By using this non-invasive approach to identify patients likely to benefit from neoadjuvant chemoimmunotherapy early, we can potentially spare those unlikely to respond to ICIs from ineffective treatment and its associated toxicity.

Abbreviations

AUC	Area under the curve
CT	Computed tomography
CI	Confidence interval
DCA	Decision curve analysis
ICIs	Immune checkpoint inhibitors
IDI	Integrated discrimination improvement
LASSO	Least absolute shrinkage and selection operator
LNs	Lymph nodes
MPR	Major pathological response
NPV	Negative predictive value
NRI	Net reclassification improvement

NSCLC	Non–small cell lung cancer
OR	Odds ratios
pCR	Pathological complete response
PD–L1	Programmed death–ligand 1
PET	Positron emission tomography
PD	Progression–free disease
PPV	Positive predictive value
SHAP	SHapley Additive exPlanations
SUVmax	Maximum standardised uptake value
VOIs	Volumes of interest

Acknowledgements
None.

Author contributions
WX and XL conceived and designed this study. XL, LL, and LZ made the doctor diagnosis, conducted the pathology analysis, and performed image segmentation. XL, QS, and ZJ conducted the statistical analysis. The origin draft of the manuscript was written by XL and QS. All authors read and approved the final manuscript.

Funding
This work was supported by grants from the National Natural Science Foundation of China (No. 82102133) and Tianjin Key Medical Discipline(Specialty) Construction Project（TJYXZDXK009A）.

Data availability
The data used and/or analyzed during the current study are available from the corresponding author on reasonable request.

Declarations

Ethics approval and consent to participate
The study was approved by the Ethics Committee of Tianjin Medical University Cancer Hospital (Approval number: bc20241623). The need for informed consent was waived by the Ethics Committee of Tianjin Medical University Cancer Hospital due to the retrospective study design. The study was conducted in accordance with the ethical principles outlined in the Declaration of Helsinki.

Consent for publication
Not applicable.

Competing interests
The authors declare no competing interests.

Author details
[1]Department of Molecular Imaging and Nuclear Medicine, Tianjin Medical University Cancer Institute and Hospital, National Clinical Research Center for Cancer, Huanhuxi Road, Hexi Distinct, Tianjin 300060, China
[2]Department of Radiology, Tianjin Hospital, Jiefangnan Road, Hexi District, Tianjin 300211, China
[3]Tianjin's Clinical Research Center for Cancer, Tianjin 300060, China
[4]Key Laboratory of Cancer Prevention and Therapy, Tianjin, China

Received: 5 December 2024 / Accepted: 10 March 2025
Published online: 21 March 2025

References

1. Waldman AD, Fritz JM, Lenardo MJ. Guide to cancer immunotherapy: from T cell basic T-cell science to clinical practice. Nat Rev Immunol. 2020;20:651–68.
2. West H, McCleod M, Hussein M, Morabito A, Rittmeyer A, Conter HJ, et al. Atezolizumab in combination with carboplatin plus nab-paclitaxel chemotherapy compared with chemotherapy alone as a first-line treatment for metastatic non-squamous non-small-cell lung cancer (IMpower130): A multicenter, randomized, open-label, phase 3 trial. Lancet Oncol. 2019;20:924–37.
3. Mok TSK, Wu Y-L, Kudaba I, Kowalski DM, Cho BC, Turna HZ, et al. Pembrolizumab versus chemotherapy for previously untreated, PD-L1-expressing, locally advanced, or metastatic non-small-cell lung cancer (KEYNOTE-042): A randomized, open-label, controlled, phase 3 trial. Lancet. 2019;393:1819–30.
4. Sorin M, Prosty C, Ghaleb L, Nie K, Katergi K, Shahzad MH, et al. Neoadjuvant chemoimmunotherapy for NSCLC: A systematic review and meta-analysis. JAMA Oncol. 2024;10:621–33.
5. Liu J, Blake SJ, Yong MCR, Harjunpää H, Ngiow SF, Takeda K, et al. Improved efficacy of neoadjuvant therapy compared to adjuvant immunotherapy in eradicating metastatic disease. Cancer Discov. 2016;6:1382–99.
6. Salmon H, Idoyaga J, Rahman A, Leboeuf M, Remark R, Jordan S, et al. Expansion and activation of CD103(+) dendritic cell progenitors at the tumor site enhance tumor responses to therapeutic PD-L1 and BRAF Inhibition. Immunity. 2016;44:924–38.
7. Lavin Y, Kobayashi S, Leader A, Amir ED, Elefant N, Bigenwald C, et al. Innate immune landscape in early lung adenocarcinoma using paired single-cell analysis. Cell. 2017;169:750–e76517.
8. Felip E, Altorki N, Zhou C, Csőszi T, Vynnychenko I, Goloborodko O, et al. Adjuvant atezolizumab after adjuvant chemotherapy in resected stage IB–IIIA non-small-cell lung cancer (IMpower010): a randomized, multicenter, open-label, phase 3 trial. Lancet. 2021;398:1344-57.
9. Paz-Ares L, O'Brien MER, Mauer M, Dafni U, Oselin K, Havel L, et al. VP3-2022: pembrolizumab (pembro) versus placebo for early-stage non-small cell lung cancer (NSCLC) following complete resection and adjuvant chemotherapy (chemo) when indicated: randomized, triple-blind, phase III EORTC-1416-LCG/ETOP 8–15– PEARLS/KEYNOTE-091 study. Ann Oncol. 2022;33:451–3.
10. Hellmann MD, Chaft JE, William WN Jr., Rusch V, Pisters KMW, Kalhor N, et al. Pathological response after neoadjuvant chemotherapy in resectable non-small-cell lung cancers: proposal for the use of major pathological response as a surrogate endpoint. Lancet Oncol. 2014;15:e42–50.
11. Pataer A, Kalhor N, Correa AM, Raso MG, Erasmus JJ, Kim ES, et al. Histopathologic response criteria predict survival of patients with resected lung cancer after neoadjuvant chemotherapy. J Thorac Oncol. 2012;7:825–32.
12. Fayanju OM, Ren Y, Thomas SM, Greenup RA, Plichta JK, Rosenberger LH, et al. The clinical significance of breast-only and node-only pathologic complete response (pCR) after neoadjuvant chemotherapy (NACT): A review of 20,000 breast cancer patients in the National cancer data base (NCDB). Ann Surg. 2018;268:591–601.
13. Chaft JE, Rusch V, Ginsberg MS, Paik PK, Finley DJ, Kris MG, et al. Phase II trial of neoadjuvant bevacizumab plus chemotherapy and adjuvant bevacizumab in patients with resectable nonsquamous Non–Small-cell lung cancers. J Thorac Oncol. 2013;8:1084-90.
14. Provencio M, Calvo V, Romero A, Spicer JD, Cruz-Bermúdez A. Treatment sequencing in resectable lung cancer: the good and the bad of adjuvant versus neoadjuvant therapy. Am Soc Clin Oncol Educ Book. 2022;42:1–18.
15. Kumagai S, Togashi Y, Kamada T, Sugiyama E, Nishinakamura H, Takeuchi Y, et al. The PD-1 expression balance between effector and regulatory T cells predicts the clinical efficacy of PD-1 Blockade therapies. Nat Immunol. 2020;21:1346–58.
16. Meng X, Huang Z, Teng F, Xing L, Yu J. Predictive biomarkers in PD-1/PD-L1 checkpoint Blockade immunotherapy. Cancer Treat Rev. 2015;41:868–76.
17. Deng H, Zhao Y, Cai X, Chen H, Cheng B, Zhong R, et al. PD-L1 expression and tumor mutation burden as pathological response biomarkers of neoadjuvant immunotherapy for Early-stage non-small cell lung cancer: A systematic review and meta-analysis. Crit Rev Oncol Hematol. 2022;170:103582.
18. Krieger T, Pearson I, Bell J, Doherty J, Robbins P. Targeted literature review on use of tumor mutational burden status and programmed cell death ligand 1 expression to predict outcomes of checkpoint inhibitor treatment. Diagn Pathol. 2020;15:6.
19. Greenspan BS. Role of PET/CT for precision medicine in lung cancer: perspective of the society of nuclear medicine and molecular imaging. Transl Lung Cancer Res. 2017;6:617–20.
20. Higuchi M, Owada Y, Inoue T, Watanabe Y, Yamaura T, Fukuhara M, et al. FDG-PET in the evaluation of response to nivolumab in recurrent non-small-cell lung cancer. World J Surg Oncol. 2016;14:238.
21. Eshghi N, Lundeen TF, Kuo PH. Dynamic adaptation of tumor immune response with nivolumab demonstrated by 18F-FDG PET/CT. Clin Nucl Med. 2018;43:114–6.
22. Polverari G, Ceci F, Bertaglia V, Reale ML, Rampado O, Gallio E, et al. 18F-FDG pet parameters and radiomics features analysis in advanced Nsclc treated with immunotherapy as predictors of therapy response and survival. Cancers (Basel). 2020;12:1163.
23. Tao X, Li N, Wu N, He J, Ying J, Gao S, et al. The efficiency of (18)F-FDG PET-CT for predicting the major pathologic response to the neoadjuvant PD-1

Blockade in resectable non-small cell lung cancer. Eur J Nucl Med Mol Imaging. 2020;47:1209–19.
24. Lambin P, Rios-Velazquez E, Leijenaar R, Carvalho S, van Stiphout RGPM, Granton P, et al. Radiomics: extracting more information from medical images using advanced feature analysis. Eur J Cancer. 2012;48:441–6.
25. Hannequin P, Decroisette C, Kermanach P, Berardi G, Bourbonne V. FDG PET and CT radiomics in diagnosis and prognosis of non-small-cell lung cancer. Transl Lung Cancer Res. 2022;11:2051–63.
26. Wang X, Gong G, Sun Q, Meng X. Prediction of pCR based on clinical-radiomics model in patients with locally advanced ESCC treated with neoadjuvant chemoimmunotherapy plus chemoradiotherapy. Front Oncol. 2024;14:1350914.
27. Wang F, Yang H, Chen W, Ruan L, Jiang T, Cheng L, et al. A combined model using pre-treatment CT radiomics and clinicopathological features of non-small cell lung cancer to predict major pathological responses after neoadjuvant chemoimmunotherapy. Curr Probl Cancer. 2024;50:101098.
28. Carvalho S, Leijenaar RTH, Troost EGC, van Timmeren JE, Oberije C, van Elmpt W, et al. 18F-fluorodeoxyglucose positron-emission tomography (FDG-PET)-Radiomics of metastatic lymph nodes and primary tumor in non-small cell lung cancer (NSCLC) - A prospective externally validated study. PLoS ONE. 2018;13:e0192859.
29. Li S, Zheng Q, Ma Y, Wang Y, Feng Y, Zhao B, et al. Implications of false negative and false positive diagnosis in lymph node staging of NSCLC by means of 18F-FDG PET/CT. PLoS ONE. 2013;8:e78552.
30. Nakanishi K, Nakamura S, Sugiyama T, Kadomatsu Y, Ueno H, Goto M, et al. Diagnostic utility of metabolic parameters on FDG PET/CT for lymph node metastasis in patients with cN2 non-small cell lung cancer. BMC Cancer. 2021;21:983.
31. Dong X, Wu P, Sun X, Li W, Wan H, Yu J, et al. Intra-tumour 18F-FDG uptake heterogeneity decreases the reliability on target volume definition with positron emission tomography/computed tomography imaging. J Med Imaging Radiat Oncol. 2015;59:338–45.
32. Schmidt-Hansen M, Baldwin DR, Hasler E, Zamora J, Abraira V, Roqué I, Figuls M, et al. PET-CT for assessing mediastinal lymph node involvement in patients with suspected resectable non-small cell lung cancer. Cochrane Database Syst Rev. 2014;2014:CD009519.
33. Montemuiño Muñiz S, Marcos Sánchez S, Calzas Rodríguez J, Losada Vila B, Llorente Herrero E, Hisado Díaz MD, et al. Advances in multimodal treatment for stage IIIA-N2 non-small cell lung cancer. J Clin Transl Res. 2021;7:185–98.
34. Ling Y, Li N, Li L, Guo C, Wei J, Yuan P, et al. Different pathologic responses to neoadjuvant anti-PD-1 in primary squamous lung cancer and regional lymph nodes. NPJ Precis Oncol. 2020;4:32.
35. Waser NA, Quintana M, Schweikert B, Chaft JE, Berry L, Adam A, et al. Pathological response in resectable non-small cell lung cancer: A systematic literature review and meta-analysis. JNCI Cancer Spectr. 2024;8:pkae021.
36. Gao S, Li N, Gao S, Xue Q, Ying J, Wang S, et al. Neoadjuvant PD-1 inhibitor (Sintilimab) in NSCLC. J Thorac Oncol. 2020;15:816–26.
37. Shu CA, Gainor JF, Awad MM, Chiuzan C, Grigg CM, Pabani A, et al. Neoadjuvant Atezolizumab and chemotherapy in patients with resectable non-small-cell lung cancer: an open-label, multicentre, single-arm, phase 2 trial. Lancet Oncol. 2020;21:786–95.
38. Kim EY, Kim YS, Park I, Ahn HK, Lee HY, Kim JH. Radiologic presentation of non-small cell lung cancer treated with anti-PD-1 therapy. J Thorac Dis. 2018;10(Suppl 33):S3930–2.
39. Zhao ZR, Yang CP, Chen S, Yu H, Lin YB, Lin YB, et al. Phase 2 trial of neoadjuvant Toripalimab with chemotherapy for resectable stage III non-small-cell lung cancer. Oncoimmunology. 2021;10:1996000.
40. Zhuang F, Haoran E, Huang J, Wu J, Xu L, Zhang L, et al. Utility of 18F-FDG PET/CT uptake values in predicting response to neoadjuvant chemoimmunotherapy in resectable non-small cell lung cancer. Lung Cancer. 2023;178:20–7.
41. Yoo J, Lee J, Cheon M, Woo SK, Ahn MJ, Pyo HR, et al. Predictive value of 18F-FDG PET/CT using machine learning for pathological response to neoadjuvant concurrent chemoradiotherapy in patients with stage III non-small cell lung cancer. Cancers (Basel). 2022;14:1987.
42. Yang M, Li X, Cai C, Liu C, Ma M, Qu W, et al. [18F]FDG PET-CT radiomics signature to predict pathological complete response to neoadjuvant chemoimmunotherapy in non-small cell lung cancer: A multicenter study. Eur Radiol. 2024;34:4352–63.
43. Seban R-D, Arnaud E, Loirat D, Cabel L, Cottu P, Djerroudi L, et al. [18F]FDG PET/CT for predicting triple-negative breast cancer outcomes after neoadjuvant chemotherapy with or without pembrolizumab. Eur J Nucl Med Mol Imaging. 2023;50:4024–35.
44. Wang Y, Shen L, Wan J, Zhang H, Wu R, Wang J, et al. Neoadjuvant chemoradiotherapy combined with immunotherapy for locally advanced rectal cancer: A new era for anal preservation. Front Immunol. 2022;13:1067036.
45. Deutsch JS, Cimino-Mathews A, Thompson E, Provencio M, Forde PM, Spicer J, et al. Association between pathologic response and survival after neoadjuvant therapy in lung cancer. Nat Med. 2024;30:218–28.
46. Sun W, Qu L, Wu J, Liu X, Wang C, Jiang Y, et al. Percentage and size of residual viable tumor in lymph node, the performance in estimating pathologic response of lymph node in non-small cell lung cancer treated with neoadjuvant chemoimmunotherapy. Hum Pathol. 2024;149:1–9.
47. Ouyang ML, Wang YR, Deng QS, Zhu YF, Zhao ZH, Wang L, et al. Development and validation of a (18)F-FDG PET-Based radiomics model for evaluating hypermetabolic mediastinal-Hilar lymph nodes in Non-Small-Cell lung cancer. Front Oncol. 2021;11:710909.
48. Wang M, Liu L, Dai Q, Jin M, Huang G. Developing a primary tumor and lymph node 18F-FDG PET/CT-clinical (TLPC) model to predict lymph node metastasis of resectable T2-4 NSCLC. J Cancer Res Clin Oncol. 2023;149:247–61.
49. Chen Y, Mao B, Peng X, Zhou Y, Xia K, Guo H, et al. A comparative study of genetic profiles of key oncogenesis-related genes between primary lesions and matched lymph nodes metastasis in lung cancer. J Cancer. 2019;10:1642–50.
50. Zhang Y, Chang L, Yang Y, Fang W, Guan Y, Wu A, et al. Intratumor heterogeneity comparison among different subtypes of non-small-cell lung cancer through multi-region tissue and matched ctdna sequencing. Mol Cancer. 2019;18:7.
51. Gao Y, Bado I, Wang H, Zhang W, Rosen JM, Zhang XHF. Metastasis organotropism: redefining the congenial soil. Dev Cell. 2019;49:375–91.
52. Jin Y, Kattan MW. Methodologic issues specific to prediction model development and evaluation. Chest. 2023;164:1281–9.
53. Zhao Y, Fu J, Liu Y, Sun H, Fu Q, Zhang S, et al. Prediction of central lymph node metastasis in patients with papillary thyroid microcarcinoma by gradient-boosting decision tree model based on ultrasound radiomics and clinical features. Gland Surg. 2023;12:1722–34.
54. Yasin P, Yimit Y, Abliz D, Mardan M, Xu T, Yusufu A, et al. MRI-based interpretable radiomics nomogram for discrimination between Brucella spondylitis and pyogenic spondylitis. Heliyon. 2024;10:e23584.

Publisher's note